Inorg. Chem. **2004**, *43*, 3024–3030

Equilibrium of Low- and High-Spin States of Ni(II) Complexes Controlled by the Donor Ability of the Bidentate Ligands

Hideki Ohtsu and Koji Tanaka*

Institute for Molecular Science, CREST, Japan Science and Technology Agency (JST), 38 Nishigonaka, Myodaiji, Okazaki, Aichi 444-8585, Japan

Received December 26, 2003

Low-spin nickel(II) complexes containing bidentate ligands with modulated nitrogen donor ability, $Py(Bz)_2$ or $MePy(Bz)_2$ ($Py(Bz)_2$ = *N*,*N*-bis(benzyl)-*N*-[(2-pyridyl)methyl]amine, $MePy(Bz)_2$ = *N*,*N*-bis(benzyl)-*N*-[(6-methyl-2-pyridyl)-methyl]amine), and a β-diketonate derivative, *t*BuacacH (*t*BuacacH = 2,2,6,6-tetramethyl-3,5-heptanedione), represented as $[Ni(Py(Bz)_2)(t\text{Buacac})](PF_6)$ (**1**) and $[Ni(MePy(Bz)_2)(t\text{Buacac})](PF_6)$ (**2**) have been synthesized. In addition, the corresponding high-spin nickel(II) complexes having a nitrate ion, $[Ni(Py(Bz)_2)(t\text{Buacac})(NO_3)]$ (**3**) and $[Ni(MePy(Bz)_2)(t\text{Buacac})(NO_3)]$ (**4**), have also been synthesized for comparison. Complexes **1** and **2** have tetracoordinate low-spin square-planar structures, whereas the coordination environment of the nickel ion in **4** is a hexacoordinate high-spin octahedral geometry. The absorption spectra of low-spin complexes **1** and **2** in a noncoordinating solvent, dichloromethane (CH_2Cl_2), display the characteristic absorption bands at 500 and 540 nm, respectively. On the other hand, the spectra of a CH_2Cl_2 solution of high-spin complexes **3** and **4** exhibit the absorption bands centered at 610 and 620 nm, respectively. The absorption spectra of **1** and **2** in *N*,*N*-dimethylformamide (DMF), being a coordinating solvent, are quite different from those in CH_2Cl_2, which are nearly the same as those of **3** and **4** in CH_2Cl_2. This result indicates that the structures of **1** and **2** are converted from a low-spin square-planar to a high-spin octahedral configuration by the coordination of two DMF molecules to the nickel ion. Moreover, complex **1** shows thermochromic behavior resulting from the equilibrium between low-spin square-planar and high-spin octahedral structures in acetone, while complex **2** exists only as a high-spin octahedral configuration in acetone at any temperature. Such drastic differences in the binding constants and thermochromic properties can be ascribed to the enhancement of the acidity of the nickel ion of **2** by the steric effect of the *o*-methyl group in the $MePy(Bz)_2$ ligand in **2**, which weakens the Ni–N(pyridine) bond length compared with that of the nonsubstituted $Py(Bz)_2$ ligand in **1**.

Introduction

Control of the spin states of metal ions has attracted much attention in inorganic[1−4] and biological chemistry.[5,6] It has been of special interest to clarify how the spin states of metal ions can be controlled by external perturbation in the viewpoint of applications to molecular memories and switches.[1−4,7] In the case of nickel(II) complexes, in particular, the transformation of the nickel(II) spin state from a low-spin ($S = 0$) state with a square-planar structure to a high-spin ($S = 1$) state with an octahedral geometry is triggered by the coordination of two solvent molecules to the nickel ion, which depends on the temperature and the solvent.[1,2] Such phenomena are known as *thermochromism* and *solvatochromism*, respectively.

* To whom correspondence should be addressed. E-mail: ktanaka@ims.ac.jp.

(1) Bloomquist, D. R.; Willett, R. D. *Coord. Chem. Rev.* **1982**, *47*, 125−164.
(2) Sone, K.; Fukuda, Y. *Inorganic Thermochromism*; Springer: Berlin, 1987.
(3) Toftlund, H. *Coord. Chem. Rev.* **1989**, *94*, 67−128.
(4) (a) Gütlich, P.; Hauser, A.; Spiering, H. *Angew. Chem., Int. Ed. Engl.* **1994**, *33*, 2024−2054. (b) Gütlich, P.; Garcia, Y.; Goodwion, H. A. *Chem. Soc. Rev.* **2000**, *29*, 419−427. (c) Gütlich, P.; Garcia, Y.; Woike, T. *Coord. Chem. Rev.* **2001**, *219*−*221*, 839−879.
(5) (a) Maltempo, M. M. *J. Chem. Phys.* **1974**, *61*, 2540−2547. (b) Maltempo, M. M.; Moss, T. H.; Cusanovich, M. A. *Biochim. Biophys. Acta* **1974**, *342*, 290−305.
(6) Fujii, S.; Yoshimura, T.; Kamada, H.; Yamaguchi, K.; Suzuki, S.; Shidara, S.; Takakuwa, S. *Biochim. Biophys. Acta* **1995**, *1251*, 161−169.
(7) (a) Kahn, O.; Launay, J. P. *Chemtronics* **1988**, *3*, 140−151. (b) Kahn, O.; Kröber, J.; Jay, C. *Adv. Mater. (Weinheim, Ger.)* **1992**, *4*, 718−728.

10.1021/ic035486+ CCC: $27.50
Published on Web 04/09/2004

A number of nickel(II) complexes showing thermochromic and solvatochromic behaviors have been synthesized to explain the phenomena in terms of geometrical factors such as changes in coordination geometry.[8−13] Among those nickel(II) complexes with thermochromic and solvatochromic behaviors, however, only a few complexes have been structurally established.[13] To the best our knowledge, moreover, there has so far been no attempt to control the thermochromism and the solvatochromism, taking advantage of the donor ability of the ligands.

We report herein the synthesis, the X-ray crystal structure determination, and the electronic spectroscopic investigations of low-spin square-planar nickel(II) complexes containing bidentate ligands with modulated nitrogen donor ability, Py(Bz)$_2$ or MePy(Bz)$_2$ (Py(Bz)$_2$ = *N*,*N*-bis(benzyl)-*N*-[(2-pyridyl)methyl]amine, MePy(Bz)$_2$ = *N*,*N*-bis(benzyl)-*N*-[(6-methyl-2-pyridyl)methyl]amine),[14] and a β-diketonate derivative, *t*BuacacH (*t*BuacacH = 2,2,6,6-tetramethyl-3,5-heptanedione), represented as [Ni(Py(Bz)$_2$)(*t*Buacac)](PF$_6$) (**1**) and [Ni(MePy(Bz)$_2$)(*t*Buacac)](PF$_6$) (**2**). In addition, the corresponding high-spin octahedral nickel(II) complexes having a nitrate ion, [Ni(Py(Bz)$_2$)(*t*Buacac)(NO$_3$)] (**3**) and [Ni(MePy(Bz)$_2$)(*t*Buacac)(NO$_3$)] (**4**), have also been synthesized and the spectroscopic properties are compared with those of the low-spin complexes. The drastic difference in the solvatochromic and thermochromic behaviors accompanied by the change of spin states from $S = 0$ to $S = 1$ is observed by the comparison of the low-spin square-planar nickel(II) complexes bearing Py(Bz)$_2$ and MePy(Bz)$_2$ ligands.

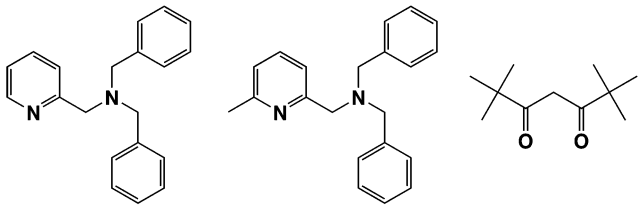

Py(Bz)$_2$ MePy(Bz)$_2$ *t*BuacacH

Experimental Section

Materials. All chemicals used for the synthesis of the ligands and complexes were commercial products of the highest available purities and were further purified by the standard methods.[15] Solvents were also purified by standard methods before use.[15]

Synthesis. All ligands used in this study were prepared according to the following procedures, and the structures of the products were confirmed by the analytical data (*vide infra*).

***N*,*N*-Bis(benzyl)-*N*-[(2-pyridyl)methyl]amine (Py(Bz)$_2$) and *N*,*N*-bis(benzyl)-*N*-[(6-methyl-2-pyridyl)methyl]amine) (MePy(Bz)$_2$).** These ligands used in this study were prepared as described previously.[14]

[Ni(Py(Bz)$_2$)(*t*Buacac)](PF$_6$) (1). To a methanol solution of Py(Bz)$_2$ (0.288 g, 1.0 mmol) and *t*BuacacH (0.184 g, 1.0 mmol) was added Ni(ClO$_4$)$_2$·6H$_2$O (0.366 g, 1.0 mmol) in methanol, and a few drops of triethylamine were then added to the resulting solution. The reaction mixture was stirred for 1 h at room temperature and concentrated to dryness under reduced pressure. The residue was dissolved in a dichloromethane solution, and ammonium hexafluorophosphate (0.326 g, 2.0 mmol) was added to the solution. After the mixture was stirred overnight at room temperature, insoluble material was removed by filtration. Addition of diethyl ether to the filtrate gradually gave red powder that was collected by filtration and recrystallized from dichloromethane/diethyl ether. Yield: 0.304 g (45.0%). Anal. Calcd for $C_{31}H_{39}O_2N_2P_1F_6Ni_1$: C, 55.14; H, 5.82; N, 4.15. Found: C, 55.02; H, 5.74; N, 4.13. Electrospray ionization (ESI) mass data: *m*/*z* 529 [M − PF$_6$]$^+$.

[Ni(MePy(Bz)$_2$)(*t*Buacac)](PF$_6$) (2). This complex was prepared in the same manner as that for the synthesis of **1** using the MePy(Bz)$_2$ ligand instead of Py(Bz)$_2$. Yield: 0.197 g (28.6%). Anal. Calcd for $C_{32}H_{41}O_{2.5}N_2P_1F_6Ni_1$: C, 55.04; H, 6.06; N, 4.01. Found: C, 55.21; H, 5.95; N, 4.07. ESI mass data: *m*/*z* 543 [M − PF$_6$]$^+$.

[Ni(Py(Bz)$_2$)(*t*Buacac)(NO$_3$)] (3). Ni(NO$_3$)$_2$·6H$_2$O (0.291 g, 1.0 mmol) in acetonitrile was added to an acetonitrile solution containing Py(Bz)$_2$ (0.288 g, 1.0 mmol) and *t*BuacacH (0.184 g, 1.0 mmol), and a few drops of triethylamine were then added to the resulting solution. The reaction mixture was stirred for 1 h at room temperature and concentrated to dryness under reduced pressure. The residue was dissolved in a dichloromethane solution and poured into diethyl ether to give pale blue powder that was collected by filtration and recrystallized from dichloromethane/diethyl ether. Yield: 0.291 g (49.2%). Anal. Calcd for $C_{31}H_{40}O_{5.5}N_3Ni_1$: C, 61.92; H, 6.70; N, 6.99. Found: C, 62.08; H, 6.71; N, 7.23. Fast atom bombardment (FAB) mass data: *m*/*z* 529 [M − NO$_3$]$^+$.

[Ni(MePy(Bz)$_2$)(*t*Buacac)(NO$_3$)] (4). This complex was prepared in the same manner as that for the synthesis of **3** using the MePy(Bz)$_2$ ligand instead of Py(Bz)$_2$. Yield: 0.306 g (50.5%). Anal. Calcd for $C_{32}H_{42}O_{5.5}N_3Ni_1$: C, 62.46; H, 6.88; N, 6.83. Found: C, 62.48; H, 6.88; N, 6.88. FAB mass data: *m*/*z* 543 [M − NO$_3$]$^+$.

X-ray Structure Determination. The syntheses of complexes **1**, **2**, and **4** afforded well-shaped crystals suitable for X-ray diffraction study. The crystals were mounted on a glass capillary. The X-ray experiments were carried out on a Rigaku/MSC mercury CCD diffractometer equipped with a Rigaku GNNP low-temperature device. Data collections were performed at 173 K under cold nitrogen gas using graphite monochromated Mo Kα radiation (λ = 0.71070 Å) and processed with Crystal Clear.[16] The structure was solved by the direct method[17] and expanded by Fourier techniques.[18] The non-hydrogen atoms were refined anisotropically by full-matrix least-squares calculations. Each refinement was

(8) (a) Ihara, Y.; Tsuchiya, R. *Bull. Chem. Soc. Jpn*. **1980**, *53*, 1614−1617. (b) Ihara, Y.; Izumi, E.; Uehara, A.; Tsuchiya, R.; Nakagawa, S.; Kyuno, E. *Bull. Chem. Soc. Jpn*. **1982**, *55*, 1028−1032. (c) Ihara, Y.; Tsuchiya, R. *Bull. Chem. Soc. Jpn*. **1984**, *57*, 2829−2831. (d) Ihara, Y. *Bull. Chem. Soc. Jpn*. **1985**, *58*, 3248−3251. (e) Ihara, Y.; Wada, A.; Fukuda, Y.; Sone, K. *Bull. Chem. Soc. Jpn*. **1986**, *59*, 2309−2315. (f) Ihara, Y.; Fukuda, Y.; Sone, K. *Inorg. Chem*. **1987**, *26*, 3745−3750.
(9) Fukuda, Y.; Sone, K. *J. Inorg. Nucl. Chem*. **1972**, *34*, 2315−2328.
(10) Vitiello, J. D.; Billo, E. J. *Inorg. Chem*. **1980**, *19*, 3477−3481.
(11) (a) Hay, R. W.; Bembi, R.; Sommerville, W. *Inorg. Chim. Acta* **1982**, *59*, 147−153. (b) Hay, R. W.; Jeragh, B.; Ferguson, G.; Kaitner, B.; Ruhl, B. L. *J. Chem. Soc., Dalton Trans*. **1982**, 1531−1539.
(12) Laskar, I. R.; Maji, T. K.; Das, D.; Lu, T.-H.; Wong, W.-T.; Okamoto, K.; Chaudhuri, N. R. *Polyhedron* **2001**, *20*, 2073−2082.
(13) Flamini, A.; Fares, V.; Pifferi, A. *Eur. J. Inorg. Chem*. **2000**, 537−544.
(14) Shimazaki, Y.; Nogami, T.; Tani, F.; Odani, A.; Yamauchi, O. *Angew. Chem., Int. Ed. Engl*. **2000**, *40*, 3859−3862.
(15) Perrin, D. D.; Armarego, W. L. F. *Purification of Laboratory Chemicals*; Butterworth-Heinemann: Oxford, England, 1988.
(16) *Crystal Clear*; software package; Rigaku and Molecular Structure Corporation: 1999.
(17) SIR92: Altomare, A.; Cascarano, G.; Giacovazzo, C.; Guagliardi, A.; Burla, M. C.; Polidori, G.; Camalli, M. *J. Appl. Crystallogr*. **1994**, *27*, 435−436.

Table 1. Crystal Data for Complexes **1**, **2**, and **4**

	1	**2**	**4**
formula	$C_{31}H_{39}N_2O_2Ni_1P_1F_6$	$C_{32}H_{41}N_2O_2Ni_1P_1F_6$	$C_{32}H_{41}N_3O_5Ni_1$
formula weight	675.33	689.35	606.39
color	red	purple	light blue
crystal size/mm	0.30 × 0.10 × 0.10	0.20 × 0.20 × 0.20	0.30 × 0.15 × 0.15
crystal system	triclinic	monoclinic	monoclinic
space group	$P\bar{1}$ (No. 2)	$C2/c$ (No. 15)	$P2_1$ (No. 4)
a/Å	10.8749(5)	21.82(1)	9.774(2)
b/Å	11.9336(5)	11.160(6)	9.712(2)
c/Å	14.6196(5)	27.91(1)	16.132(3)
α/deg	71.93(1)		
β/deg	84.55(2)	104.536(5)	96.583(9)
γ/deg	63.03(1)		
V/Å^3	1605.2(2)	6579(5)	1521.2(4)
Z	2	8	2
T/K	173	173	173
D_c/(g cm^{-3})	1.397	1.392	1.324
radiation	Mo Kα ($\lambda = 0.71070$ Å)	Mo Kα ($\lambda = 0.71070$ Å)	Mo Kα ($\lambda = 0.71070$ Å)
μ/cm^{-1}	7.19	7.04	6.82
F(000)/e	704.00	2880.00	644.00
$2\theta_{max}$/deg	55.0	55.0	55.0
no. of reflctns measd	7043	7815	3568
no. of observations	6978	7392	3562
no. of variables	388	397	371
GOF	1.88	1.74	1.28
R^a ($I > 2.00\sigma(I)$)	0.069	0.062	0.034
$R_w{}^a$ ($I > 2.00\sigma(I)$)	0.087	0.078	0.048

[a] $R = \sum(|F_o| - |F_c|)/\sum|F_o|$; $R_w = [\sum w(|F_o| - |F_c|)^2/\sum w|F_o|^2]^{1/2}$; $w = 1/\sigma^2(F_o)$.

continued until all shifts were smaller than one-third of the standard deviations of the parameters involved. Atomic scattering factors were taken from the literature.[19] All hydrogen atoms were located at the calculated positions, and they were assigned a fixed displacement and constrained to ideal geometry with C−H = 0.95 Å. All the calculations were performed by using the teXsan crystallographic software program package.[20] Summaries of the fundamental crystal data and experimental parameters for the structure determination of complexes **1**, **2**, and **4** are given in Table 1.

Instrumental Measurements. Electronic spectra were measured with a Hewlett-Packard 8453 diode array spectrophotometer with a Unisoku thermostated cell holder designed for low-temperature experiments. NMR measurements were performed with a JEOL GX-500 (500 MHz) NMR spectrometer. ESI mass spectra were obtained with a Shimadzu LCMS-2010 liquid chromatograph mass spectrometer. FAB mass spectra were recorded with a JEOL JMS-GCmateII spectrometer. Cold-spray ionization (CSI) mass spectra were taken on a JEOL JMS-T100CS spectrometer attached to a syringe pump apparatus (Harvard Apparatus model 22). Sample solutions were delivered to the sprayer through a fused silica capillary (100 μm diameter) at 10 μL/s. The sprayer was held at a potential of 2.0 kV, and compressed N_2 which controlled the temperature at 248 K was employed to assist liquid nebulization. The orifice potential was maintained at 30 V. The positive ion CSI mass spectra were measured in the range m/z = 100−1000. Variable-temperature magnetic susceptibility data were measured on polycrystalline samples of complexes **1**, **2**, **3**, and **4** using a Quantum Design MPMS-7 SQUID susceptometer in the temperature range 4−300 K with an applied field of 5.0 kG. The polycrystalline sample was embedded in Parafilm to prevent torquing of the crystallites in an external field. A diamagnetic correction, estimated from Pascal's constants,[21] was added from the experimental susceptibilities to give the molar paramagnetic susceptibilities. Elemental analyses were carried out at the Research Center for Molecular-scale Nanoscience, Institute for Molecular Science.

Results and Discussion

Crystal Structures. ORTEP views of low-spin nickel (II) complexes **1** and **2** are shown in Figure 1 (parts a and b, respectively), and that of the corresponding high-spin nickel-(II) complex **4** containing a nitrate ion is shown in Figure 2. Selected bond distances and angles of complexes **1**, **2**, and **4** are summarized in Tables 2, 3, and 4, respectively.

The nickel ions in **1** and **2** have tetracoordinate structures formed by the pyridine nitrogen, the tertiary amine nitrogen, and two oxygens from *t*Buacac. The bond lengths of **1** and **2** from the nickel ion to each of the donor nitrogens and oxygens are Ni−N(1), 1.893(3) and 1.936(2) Å; Ni−N(2), 1.944(3) and 1.949(3) Å; Ni−O(1), 1.842(3) and 1.844(2) Å; and Ni−O(2), 1.821(3) and 1.845(2) Å, respectively. It should be noted that the Ni−N(1) distance in **2** (1.936(2) Å) is significantly longer than that in **1** (1.893(3) Å). Such a difference in the Ni−N(pyridine) distance may be ascribed to the steric effect of the *o*-methyl group[22] of the MePy-$(Bz)_2$ ligand in **2**, which leads to weaker coordination to the nickel ion as compared to the case of the nonsubstituted Py-$(Bz)_2$ ligand in **1**. This is consistent with the higher value of the binding constant with DMF in **2** than in **1**, as discussed later. The dihedral angles between the Ni−N(1)−N(2) plane and the Ni−O(1)−O(2) one in **1** and **2** are 12.4 and 19.9°,

(18) DIRDIF94: Beurskens, P. T.; Admiraal, G.; Beurskens, G.; Bosman, W. P.; de Gelder, R.; Israel, R.; Smits, J. M. M. *The DIRDIF94 program system*; Crystallography Laboratory, University of Nijmegen: The Netherlands, 1994.
(19) *International Tables for X-ray Crystallography*; Kynoch Press: Birmingham, U.K., 1974; Vol. IV.
(20) *teXsan*; crystal structure analysis package; Molecular Structure Corporation: 1985 and 1999.
(21) Mabbs, F. E.; Marchin, D. J. *Magnetisms and Transition Metal Complexes*; Chapman and Hall: London, 1975.

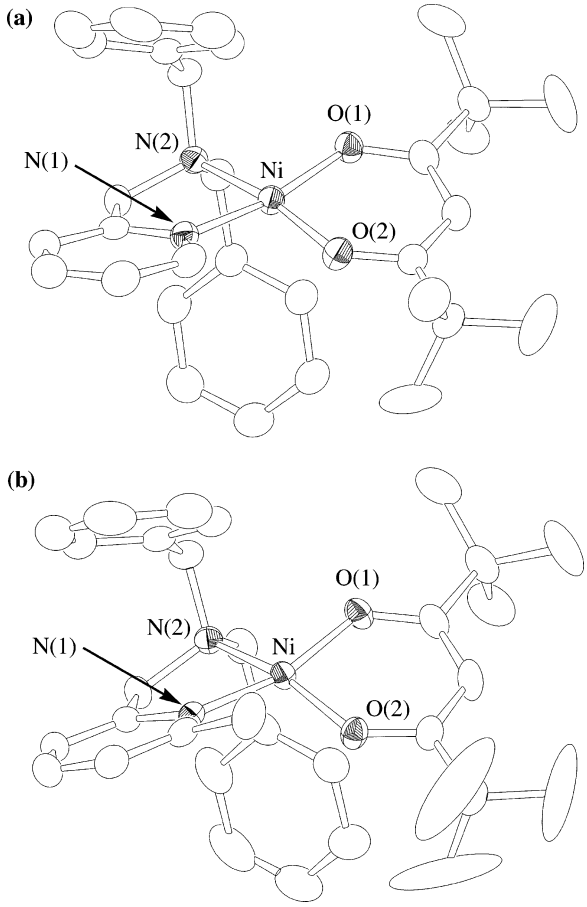

Figure 1. ORTEP views of (a) [Ni(Py(Bz)$_2$)(*t*Buacac)](PF$_6$) (**1**) and (b) [Ni(MePy(Bz)$_2$)(*t*Buacac)](PF$_6$) (**2**). The hydrogen atoms and the counteranion are omitted for clarity. Thermal ellipsoids are drawn at the 50% probability level.

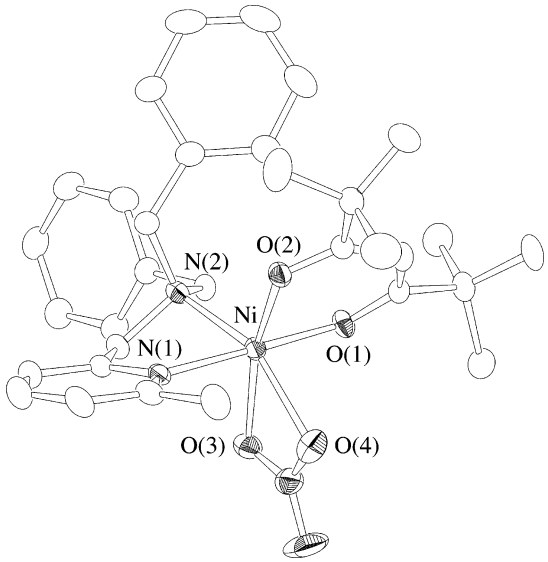

Figure 2. ORTEP view of [Ni(MePy(Bz)$_2$)(*t*Buacac)(NO$_3$)] (**4**). The hydrogen atoms are omitted for clarity. Thermal ellipsoids are drawn at the 50% probability level.

respectively. Thus, the coordination environments of **1** and **2** are slightly distorted square-planar structures, which are consistent with the magnetic susceptibilities of **1** and **2** that were diamagnetic ($S = 0$).

Table 2. Selected Bond Distances and Angles of Complex **1**

Bond Distances (Å)			
Ni−N(1)	1.893(3)	Ni−O(1)	1.842(2)
Ni−N(2)	1.944(3)	Ni−O(2)	1.821(3)
Bond Angles (deg)			
N(1)−Ni−N(2)	86.0(1)	N(2)−Ni−O(1)	89.9(1)
N(1)−Ni−O(1)	169.6(1)	N(2)−Ni−O(2)	170.5(1)
N(1)−Ni−O(2)	90.2(1)	O(1)−Ni−O(2)	95.3(1)

Table 3. Selected Bond Distances and Angles of Complex **2**

Bond Distances (Å)			
Ni−N(1)	1.936(2)	Ni−O(1)	1.844(2)
Ni−N(2)	1.949(3)	Ni−O(2)	1.845(2)
Bond Angles (deg)			
N(1)−Ni−N(2)	85.7(1)	N(2)−Ni−O(1)	88.39(10)
N(1)−Ni−O(1)	165.5(1)	N(2)−Ni−O(2)	164.3(1)
N(1)−Ni−O(2)	94.38(10)	O(1)−Ni−O(2)	94.87(9)

Table 4. Selected Bond Distances and Angles of Complex **4**

Bond Distances (Å)			
Ni−N(1)	2.086(3)	Ni−O(2)	1.979(2)
Ni−N(2)	2.184(2)	Ni−O(3)	2.120(2)
Ni−O(1)	1.983(2)	Ni−O(4)	2.182(3)
Bond Angles (deg)			
N(1)−Ni−N(2)	80.9(1)	N(2)−Ni−O(4)	152.34(10)
N(1)−Ni−O(1)	177.23(9)	O(1)−Ni−O(2)	91.10(8)
N(1)−Ni−O(2)	90.7(1)	O(1)−Ni−O(3)	88.1(1)
N(1)−Ni−O(3)	90.70(9)	O(1)−Ni−O(4)	87.8(1)
N(1)−Ni−O(4)	93.75(10)	O(2)−Ni−O(3)	164.22(9)
N(2)−Ni−O(1)	96.67(9)	O(2)−Ni−O(4)	103.99(9)
N(2)−Ni−O(2)	103.20(10)	O(3)−Ni−O(4)	60.23(9)
N(2)−Ni−O(3)	92.55(9)		

The transformation from low-spin square-planar complexes **1** and **2** to the corresponding high-spin octahedral complexes was demonstrated by the 1:1 adduct formation with a nitrate ion affording **3** and **4**, respectively (see the Experimental Section), and well-shaped crystals suitable for X-ray structure determination were obtained in the case of **4**. The coordination geometry of the nickel ion in **4** is an octahedral structure with two nitrogens of the pyridine and the tertiary amine, two oxygens from *t*Buacac, and two oxygens of the nitrate ion bonded in the bidentate manner, as shown in Figure 2. The bond lengths and angles around the nickel coordination sphere of **4** (see Table 4) are essentially the same as those of the reported complex [Ni(dipe)(acac)(NO$_3$)].[23,24] Thus, the structure of **3** is also quite similar to those of **4** and [Ni(dipe)(acac)(NO$_3$)],[23,24] with respect to the coordination geometry. In addition, the effective magnetic moments of **3**, **4**, and [Ni(dipe)(acac)(NO$_3$)][23,24] were 3.20, 3.02, and 3.23 μ_B, respectively,[23,25] indicating that the spin states of the nickel ions in these complexes are high-spin states ($S = 1$).

Absorption Spectra in Noncoordinating and Coordinating Solvents. Parts a and b of Figure 3 show the

(22) (a) Nagao, H.; Komeda, N.; Mukaida, M.; Suzuki, M.; Tanaka, K. *Inorg. Chem.* **1996**, *35*, 6809−6815. (b) Shimazaki, Y.; Huth, S.; Hirota, S.; Yamauchi, O. *Bull. Chem. Soc. Jpn.* **2000**, *73*, 1187−1195. (c) Ohtsu, H.; Shimazaki, Y.; Odani, A.; Yamauchi, O.; Itoh, S.; Fukuzumi, S. *J. Am. Chem. Soc.* **2000**, *122*, 5733−5741. (d) Ohtsu, H.; Itoh, S.; Nagatomo, S.; Kitagawa, T.; Ogo, S.; Watanabe, Y.; Fukuzumi, S. *Inorg. Chem.* **2001**, *40*, 3200−3207. (e) Ohtsu, H.; Fukuzumi, S. *Chem. Lett.* **2001**, 920−921.
(23) Fukuda, Y.; Fujita, C.; Miyamae, H.; Nakagawa, H.; Sone, K. *Bull. Chem. Soc. Jpn.* **1989**, *62*, 745−752.
(24) dipe = 1,2-dipiperidinoethane, acac = acetylacetonate.

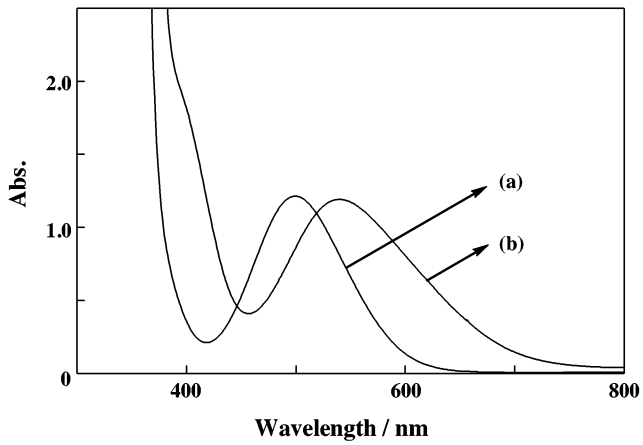

Figure 3. Absorption spectra of (a) [Ni(Py(Bz)$_2$)(*t*Buacac)](PF$_6$) (**1**: 10.0 mM) and (b) [Ni(MePy(Bz)$_2$)(*t*Buacac)](PF$_6$) (**2**: 10.0 mM) in CH_2Cl_2 at 298 K.

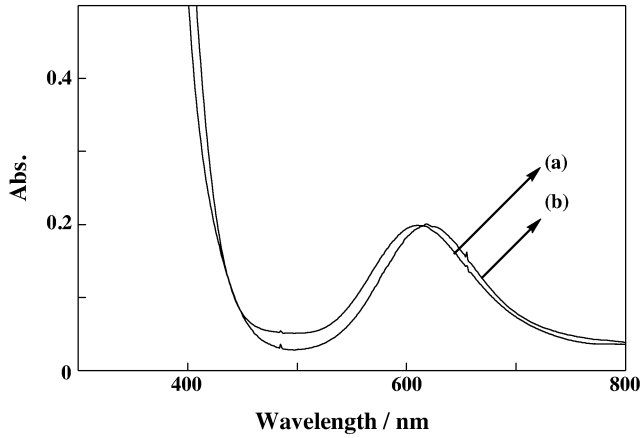

Figure 4. Absorption spectra of (a) [Ni(Py(Bz)$_2$)(*t*Buacac)(NO$_3$)] (**3**: 10.0 mM) and (b) [Ni(MePy(Bz)$_2$)(*t*Buacac)(NO$_3$)] (**4**: 10.0 mM) in CH_2Cl_2 at 298 K.

absorption spectra of **1** and **2**, respectively, in dichloromethane (CH_2Cl_2), which is a noncoordinating solvent. An intense absorption band at 500 nm ($\epsilon = 120$ M^{-1} cm^{-1}) of **1** (Figure 3a) can be assigned to the d−d transition ($^1A_{1g} \rightarrow {}^1A_{2g}$),[26] which is characteristic of low-spin square-planar nickel(II) complexes. This is consistent with the results of X-ray crystal structure determination and magnetic susceptibility. The absorption spectrum of a CH_2Cl_2 solution of **2** (Figure 3b) displays the $^1A_{1g} \rightarrow {}^1A_{2g}$ transition band[26] at 540 nm ($\epsilon = 120$ M^{-1} cm^{-1}) which is red-shifted compared to that of **1** (500 nm, $\epsilon = 120$ M^{-1} cm^{-1}).

The absorption spectra of the corresponding high-spin complexes **3** and **4** having a hexacoordinate octahedral structure in CH_2Cl_2 are shown in parts a and b of Figure 4, respectively. The spectra of **3** and **4** exhibit prominent bands centered at 610 and 620 nm ($\epsilon = 20$ M^{-1} cm^{-1} in both complexes), respectively, and the absorption coefficient of **4** is slightly red-shifted compared to that of **3**. These characteristic bands at ~600 nm are assigned to the d−d

(25) The effective magnetic moments of **3** and **4** are independent of the measured temperature range (4−300 K).

(26) Lever, A. B. P. *Inorganic Electronic Spectroscopy*, 2nd ed.; Elsevier Science: Amsterdam, The Netherlands, 1984.

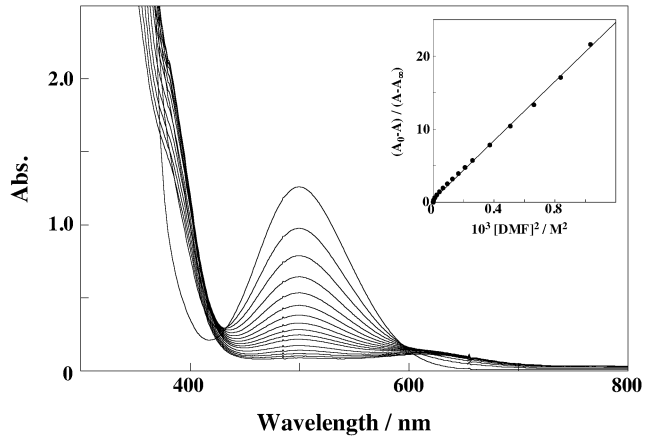

Figure 5. Absorption spectral change observed upon addition of various amounts of DMF into a CH_2Cl_2 solution of [Ni(Py(Bz)$_2$)(*t*Buacac)](PF$_6$) (**1**: 10.0 mM) at 298 K. Inset: plot of $(A_0 - A)/(A - A_\infty)$ vs [DMF]^2.

bands due to $^3A_{2g} \rightarrow {}^3T_{1g}$ (F) transitions.[26] Such a difference in the absorption maxima between **1** and **2** or between **3** and **4** may be caused by the steric effect of the *o*-methyl group of the pyridine moiety. In addition, the reflectance spectra of **1**, **2**, **3**, and **4** in the solid states showed the same bands, indicating that the structures of **1**, **2**, **3**, and **4** are maintained in the solution states.

The absorption spectra of **1** and **2** completely change when a coordinating solvent, *N*,*N*-dimethylformamide (DMF), has been used instead of a noncoordinating solvent, CH_2Cl_2. The $^3A_{2g} \rightarrow {}^3T_{1g}$ (F) transition bands of **1** and **2** in DMF appeared at λ_{max} (ϵ/(M^{-1} cm^{-1})) = 630 (20) and 645 (20) nm, respectively, which are quite close to those of **3** and **4** in CH_2Cl_2, as shown in Figure 4. This result indicates that the structures of **1** and **2** are transformed from a low-spin square-planar to a high-spin octahedral configuration because of the coordination of two DMF molecules to the tetradentate square-planar nickel ion. Formation of the 1:2 DMF adducts has been further confirmed by the CSI mass spectrum of **1** in DMF, which exhibited a signal at $m/z = 677$. The observed mass and isotope patterns correspond to the ion [Ni(Py(Bz)$_2$)(*t*Buacac)(DMF)$_2$]$^+$.

As expected from the solvatochromic properties of **1** and **2**, the spectral changes can be observed upon gradual addition of DMF into a CH_2Cl_2 solution of **1** and **2**, as shown in Figures 5 and 6. The absorption bands at 500 (for **1**) and 540 nm (for **2**) characteristic of the nickel(II) low-spin square-planar complexes decrease with increasing the concentration of added DMF, accompanied by increases in the absorption bands at 615 and 635 nm, respectively, which belong to the corresponding high-spin octahedral DMF adducts. Such spectral changes are reasonably associated with the 1:2 complex formation between **1** or **2** and DMF, as shown in Scheme 1.[27] The binding constants (K_b) for the 1:2 adducts with DMF expressed by eq 1 are calculated by using the equation

$$K_b = [\text{Ni(L)}(t\text{Buacac})(\text{DMF})_2]/[\text{Ni(L)}(t\text{Buacac})]\,[\text{DMF}]^2 \quad (1)$$

$$\text{L} = \text{Py(Bz)}_2 \text{ or MePy(Bz)}_2$$

Scheme 1

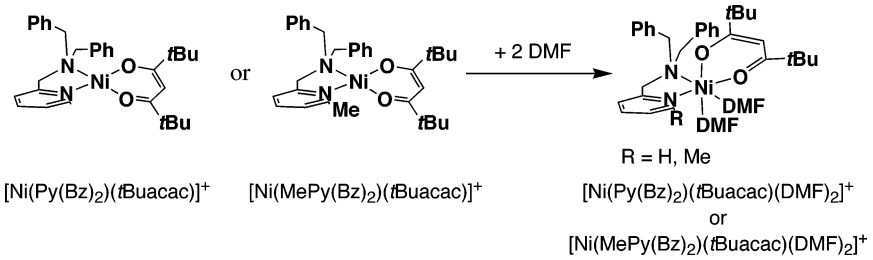

Scheme 2

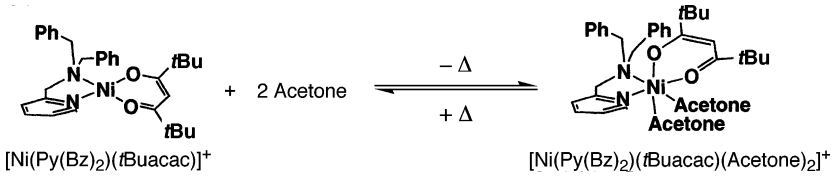

$(A_0 - A)/(A - A_\infty) = 0.01K_b[\mathrm{DMF}]^2$. The plots of $(A_0 - A)/(A - A_\infty)$ versus $[\mathrm{DMF}]^2$ give straight lines passing through the origin, as depicted in the insets of Figures 5 and 6. The K_b values are determined as 0.20 and 930 M^{-1} for **1** and **2**, respectively, from the slopes of the plots. The significantly larger binding constant of **2** compared with that of **1** indicates that the *o*-methyl group of the $MePy(Bz)_2$ ligand greatly enhances the acidity of the nickel ion. This is consistent with the longer Ni−N(pyridine) distance in **2** (1.936(2) Å) than in **1** (1.893(3) Å), derived from the crystal structures (*vide supra*). Such a drastic difference of K_b values in **1** and **2** reflects the thermal behavior of both complexes as described in the next section.

Thermochromic Properties. We observed that complexes **1** and **2** display very different thermal behaviors in acetone, which is a weaker coordinating solvent as compared to DMF. The absorption spectrum of **1** in acetone at room temperature is quite close to that in CH_2Cl_2 (see Figure 3a) and exhibits the $^1A_{1g} \rightarrow {}^1A_{2g}$ transition band[26] at 500 nm. Upon cooling an acetone solution of **1** down to 183 K, however, the color gradually changes from red ($\lambda_{max} = 500$ nm) toward pale blue ($\lambda_{max} = 610$ nm), as shown in Figure 7. The remarkable thermochromism is associated with the reversible temperature-dependent change between the low-spin square-planar and high-spin octahedral structures. Reliable magnetic susceptibility of **1** in acetone, however, was not obtained because of the low solubility of the complex at low temperature. The spectral change depending on the temperature can be reasonably explained by the shift of the equilibrium to the right with decreasing temperature (Scheme 2).

Indeed, the absorption spectrum of **1** in acetone at 183 K is quite close to that in the presence of DMF in CH_2Cl_2 (Figure 5). On the other hand, the absorption spectrum of **2** in acetone displayed only the 630 nm band arising from the high-spin octahedral configuration at room temperature, and no spectral change was observed upon cooling the solution down to 183 K.

In contrast to the case of **1**, the lack of thermochromism in an acetone solution of **2** apparently results from too strong an affinity of the nickel ion for acetone. The distinct difference in the thermochromic behavior between **1** and **2** is associated with the binding constants of **1** and **2** with DMF, $K_b = 0.20$ and 930 M^{-1}, respectively (*vide supra*). Thus, the *o*-methyl group of the pyridine moiety in **2** plays the key role in developing thermochromism as well as solvato-

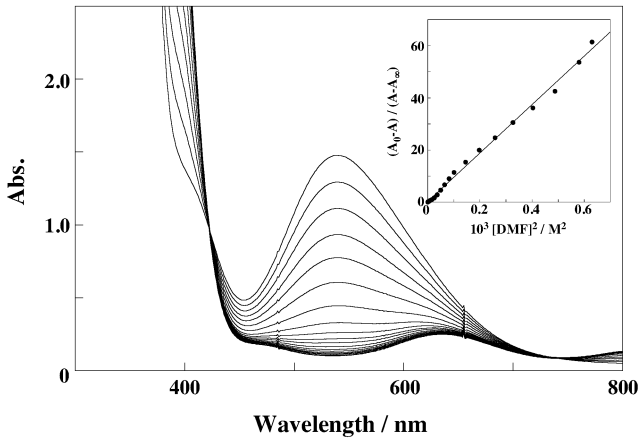

Figure 6. Absorption spectral change observed upon addition of various amounts of DMF into a CH_2Cl_2 solution of $[Ni(MePy(Bz)_2)(tBuacac)](PF_6)$ (**2**: 10.0 mM) at 298 K. Inset: plot of $(A_0 - A)/(A - A_\infty)$ vs $[DMF]^2$.

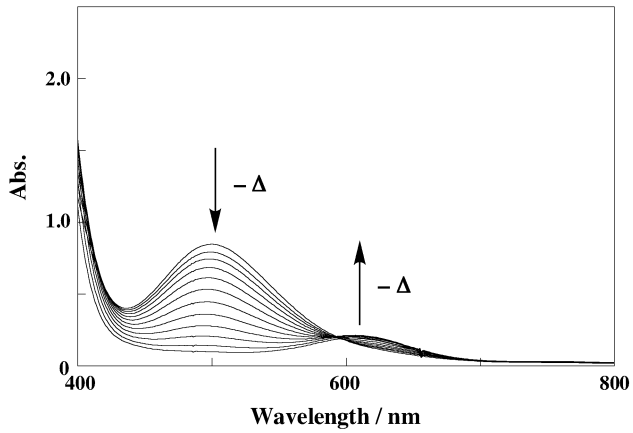

Figure 7. Absorption spectral change observed by decreasing the temperature from 298 to 183 K in an acetone solution of $[Ni(Py(Bz)_2)(tBuacac)](PF_6)$ (**1**: 10.0 mM).

chromism by weakening the Ni−N(pyridine) bond at a certain level compared with the case of the nonsubstituted $Py(Bz)_2$ ligand in **1**.

Conclusions

The low-spin square-planar nickel(II) complexes $[Ni(Py(Bz)_2)(t\text{Buacac})](PF_6)$ (**1**) and $[Ni(MePy(Bz)_2)(t\text{Buacac})](PF_6)$ (**2**), having bidentate ligands with modulated nitrogen donor ability and β-diketonate derivatives, exhibit the unique solvatochromism as well as the thermochromism induced by the change of the spin states of the nickel(II) ion from the square-planar low-spin ($S = 0$) to the octahedral high-spin ($S = 1$) states. The binding constants of **1** and **2** for the 1:2 adduct formation with DMF are determined as 0.20 and 930 M^{-1}, respectively, by the titration upon addition of DMF into a CH_2Cl_2 solution of **1** and **2**. The significantly larger binding constant of **2** compared with that of **1** clearly indicates that the steric effect of the *o*-methyl group of the $MePy(Bz)_2$ ligand greatly enhances the affinity of the central Ni(II) ion toward coordinating molecules. As a result, an acetone solution of **2** exists as octahedral high-spin $[Ni(MePy(Bz)_2)(t\text{Buacac})(acetone)_2]^+$ in a wide range of temperatures. On the other hand, complex **1** maintains the low-spin square-planar geometry ($[Ni(Py(Bz)_2)(t\text{Buacac})]^+$) in acetone at room temperature, but the molecular structure of **1** gradually changes to octahedral high-spin $[Ni(Py(Bz)_2)(t\text{Buacac})(acetone)_2]^+$ with decreasing temperature. Thus, control of the spin states in nickel(II) complexes can be accomplished by fine-tuning of the donor abilities of the ligands. The present results will provide valuable information for the development of molecular memories and switches.[1−4,7]

Acknowledgment. We are grateful to JEOL Ltd. for CSI mass measurements.

Supporting Information Available: X-ray crystallographic file in CIF format for complexes **1**, **2**, and **4**. This material is available free of charge via the Internet at http://pubs.acs.org.

IC035486+

(27) The octahedral diaqua-complex $[Ni(en)_2(H_2O)_2]^{2+}$ (en = ethylenediamine) favors the *cis* configuration as compared to the *trans* one in the solution state: Farago, M. E.; James, J. M.; Trew, V. C. G. *J. Chem. Soc. A* **1967**, 820−824. In the case of the DMF adducts with **1** and **2**, the type of coordination has yet to be determined.